Atomic layer fluorination of 5 V class positive electrode material $LiCoPO_4$ for enhanced electrochemical performance

Sanghoon Kim,[a] Eun Jeong Kim,[b,c] Youn Charles-Blin,[a,e,g] Katia Guérin,[d] Marc Dubois,[d] Delphine Flahaut,[e,g] Herve Martinez,[e,g] Michaël Deschamps,[f,g] David N. Miller,[b] John T.S. Irvine,[b] A. Robert Armstrong,[b,c] Laure Monconduit,[a,c,g] and Nicolas Louvain[a,c,g,]*

Dr S. Kim, Dr. Charles-Blin, Dr L. Monconduit, Dr N. Louvain
Institut Charles Gerhardt Montpellier, Université de Montpellier, CNRS, 34090 Montpellier, France
Dr E. J. Kim, Dr D. N. Miller, Prof. J. T. S. Irvine, Dr A. R. Armstrong
School of Chemistry, University of St Andrews, St Andrews, Fife, KY16 9ST, United Kingdom
Dr E. J. Kim, Dr A. R. Armstrong, Dr L. Monconduit, Dr N. Louvain
ALISTORE-ERI, 80039, Amiens Cedex, France
Dr K. Guérin, Prof. Marc Dubois
Université Clermont Auvergne, CNRS, Sigma Clermont, ICCF, 63000 Clermont-Ferrand, France
Dr Y. Charles-Blin, Dr D. Flahaut, Prof. H. Martinez
Université de Pau et des Pays de l'Adour, IPREM, CNRS UMR 5254, 2 avenue du président Angot, 64053 Pau Cedex
Prof. M. Deschamps
CEMHTI, CNRS UPR 3079, Université d'Orléans, F45071 Orléans, France
Dr Y. Charles-Blin, Dr D. Flahaut, Prof. H. Martinez, Prof. M. Deschamps, Dr L. Monconduit, Dr N. Louvain
Réseau sur le Stockage Electrochimique de l'Energie (RS2E), CNRS FR3459, 33 Rue Saint Leu, 80039 Amiens Cedex, France

E-mail: nicolas.louvain@umontpellier.

Keywords: LCP, fluorination, X-ray photoelectron spectroscopy (XPS), lithium ion battery

Abstract

The surface fluorination of lithium cobalt phosphate ($LiCoPO_4$, LCP) using a one-step, room temperature processable, easily up-scalable and dry surface modification method with XeF_2 as fluorine source was developed. After fluorination, fluorine-rich nanoparticles were observed mainly on the particle surface, which facilitates the improvement of surface stability and electrochemical performance such as cycling stability and rate capability, as the fluorinated LCP can be protected against side reactions with electrolyte or by-products of electrolyte decomposition at high voltage (5 V). More importantly, the direct surface fluorination proved more efficient than adding a fluorinated electrolyte additive (i.e. FEC). These results suggest

that surface fluorination using XeF_2 is of great promise for practical applications of high voltage positive materials for lithium ion batteries.

1. Introduction

With increasing need for power sources in the application of energy storage, electronic devices and electric vehicles, the improvement of power density of lithium ion batteries is in great demand.[1,2] A general approach to achieve high energy density for lithium ion batteries is to adopt high-voltage positive electrode materials, with working voltage higher than currently used cathode materials such as $LiCoO_2$ (4.2 V vs Li^+/Li).[3] However, the practical use of high-voltage positive electrode materials is still challenging, as their working voltage (5 V vs Li^+/Li) is close to the oxidation potential of the conventional organic electrolytes,[4,5] which results in the continuous degradation of the electrolyte. In addition, owing to the high working voltage, the passivating cathode electrolyte interface (CEI) would not be stable,[6,7,8] leading to the degradation of the electrode materials, including dissolution of metal ions or surface amorphization.[9]

Among different potential candidates for positive electrodes, the olivine $LiCoPO_4$ (LCP) has attracted much attention as it can deliver high energy density owing to its high redox potential (~ 4.8 V vs Li^+/Li).[10] However, practical implementation of LCP technology has been hampered by its unsatisfactory electrochemical performance associated with poor cycling stability and low rate capability, mainly due to the formation of undesired products on the surface of LCP,[11] following the structural degradation of LCP by HF present in the electrolyte[12] as well as the increase in the number of anti-site defects.[13,14] Over the years, many efforts have been made to mitigate these problems, such as metal doping[15] in the LCP crystal structure, surface coating[16] and nanostructuring.[17] In addition, the use of additives in the electrolyte,[18,19] the modification of separator[20] and the use of water soluble binders[21] have proved to be effective.

In this regard, here we report the surface fluorination of LCP using a one-step, room temperature processable, easily up-scalable and dry surface modification method with a solid-state fluorinating agent, xenon difluoride, as fluorine source. The cobalt-oxygen (Co–O) bonds at the LCP particle surface were partially replaced with cobalt–fluorine (C–F) bonds, which improved both crystal structure stability and surface stability.[22] The fluorinated LCP showed significantly enhanced electrochemical performance such as cycling stability, rate capability, and is of great promise for practical applications.

2. Results and discussion

2.1. Characterization of fluorinated LCP

Surface fluorination of LCP was performed using a one step, rapid, easily up-scalable and dry method, which relies on the sublimation of XeF_2 as fluorine source. Two surface-fluorinated LCP samples were prepared, LCP-F1 for 1h 30 and LCP-F2 for 3h 30 as reaction time, respectively.

Powder X-ray diffraction patterns of pristine and fluorinated $LiCoPO_4$ (LCP) samples were recorded with Mo $K\alpha_{1,2}$ radiation (λ = 0.7107 Å). As shown in Figure 1.a-c, diffraction peaks can be fully indexed on an orthorhombic olivine structure, where PO_4 tetrahedral and CoO_6 octahedral share corners and lithium ions occupy edge-shared octahedral sites, (space group *Pnma*) with no additional peaks, indicating that a single-phase LCP was obtained. In addition, no secondary phase is observed in the PXRD patterns, confirming the LCP phase in the bulk is largely unaffected by the fluorination. The refined results using the Le Bail method are presented in Figure 1.d-g and Table S1. The cell parameters for LCP-F1 decrease significantly, which could reflect partial substitution of F^- for O^{2-} as the radii of F^- ions (1.31 Å for four-fold coordination and 1.33 Å for six-fold coordination) are smaller compared to those of O^{2-} (1.38 Å for four-fold coordination and 1.40 Å for six-fold coordination). When LCP was subjected to longer exposure to XeF_2 (LCP-F2), the cell parameter *c* increased along

with a slight increase in *b* and a small decrease in *a*. This observation could originate from the emergence of a new phase containing F^-, which is undetectable with diffraction methods. SEM images (Figure 2a-b) reveal that the pristine LCP consists of the agglomeration of sub-micron hexagonal platelets with a thickness of around 100–150 nm, which is in good agreement with previously reported papers.[23,24] After fluorination the particle surface of LCP was modified with the appearance of a few nanoparticles (LCP-F1, Figure 2c), which became bigger on more prolonged exposure to XeF_2 (LCP-F2, Figure 2d).

In order to investigate this, scanning transmission electron microscopy (STEM) with energy dispersive X-ray (EDX) spectra of LCP-F2 particles were collected. Consistent with the SEM image, nanoparticles on the bulk particle surface are observed, which clearly demonstrates surface modification (Figure 3a). EDX spectra (Figure 3d) recorded from the surface (area 1) to the core (area 2), display the presence of fluorine, the proportion of which decreases as a function of depth. This indicates that F is mainly located on the surface and may be associated with the nanoparticles on the surface.

The composition of the nanoparticles or their crystal structure could not be determined using STEM, not only due to the size (less than 5 nm) but also the instability of these nanoparticles under the high voltage electron beam. From magnetic property measurements (Figure S1), it can be postulated that a new Co^{2+}-F bond was formed, which exhibits antiferromagnetic properties at low temperatures.

Solid-state ^{19}F, ^{7}Li and ^{31}P NMR experiments indirectly confirm the previous hypothesis of a new fluoride phase involving Co^{2+} with a different magnetic behavior from LCP (Figure S2). Indeed, while the ^{31}P NMR signature is consistent with the $LiCoPO_4$ structure and is identical for all samples, which indicates an unmodified LCP structure for LCP, LCP-F1 and LCP-F2, the ^{7}Li NMR chemical shift is deshielded by approximately 6 ppm, and so is the ^{19}F signal of the internal reference, PTFE, expected at -123 ppm but appearing at -117 ppm. This behavior,

along with enlarged ^{19}F NMR signal for PTFE most probably hiding the Li-F environments, tends to indicate a new Co-based magnetic phase disturbing the NMR signals.

To provide a closer insight of the surface chemistry, XPS analyses were carried out on pristine and fluorinated LCP nanoparticles. The total amount of fluorine is quantified up to 9.4 at% for LCP-F1 and 31.0 at% for LCP-F2, which represents nearly a third of the surface composition. Fluorine reaction with the lithium is identified as the main reactive site on the surface by the F1s component located at 685.4 eV (figure 4 a). The LiF environments are highly promoted by thermodynamics but also by the particularly high lithium mobility within the olivine structure. Indeed, the increasing fluorine content on surface is accompanied by higher lithium content. The lithium increases from 12.3 at% in the pristine compound to 18.5 at% and 33.1 at% for F1 and F2 respectively (figure 4 b). The Li(1s)/Co(2p) ratio is 1.3 for the starting LCP, after the fluorination the ratio increases to 1.9 for F1 and jumps to 13.4 for F2, highlighting a strong surface modification. Moreover, for LCP-F1, the LiF environment is accounting for 4.9 at% and for LCP-F2 it is accounting for 21.9 at%. The remaining Li1s quantities originating from the fluorinated LCP compound are in good agreement with the pristine LCP, testifying that the LCP stoichiometry is preserved beneath the fluorinated layer. The morphology observed on fluorinated nanoparticles can be related to the lithium migration towards the surface. A minority of fluorophosphate species are formed (Figure S3) while the cobalt spectra exhibit unmodified Co^{2+} signal for all the compounds.

2.2. Electrochemical performance of fluorinated LCP

The electrochemical performance of fluorinated and pristine LCP was investigated by galvanostatic cycling in a half- cell configuration using lithium metal as counter and reference electrode. Figure5a shows the cycling performance of these LCP samples over 30 cycles at 0.1 C (16.7 mA g^{-1}). The pristine LCP shows a rapid discharge capacity decrease from 102 mAh g^{-1} to 54 mAh g^{-1} with 51 % capacity retention after 30 cycles, whereas both fluorinated

LCP samples exhibit better capacity retention 79 % (117 mAh g^{-1} to 92 mAh g^{-1}) and 77 % (104 mAh g^{-1} to 80 mAh g^{-1}) for LCP-F1 and LCP-F2, respectively. This improved performance suggests that the surface fluorination may protect the LCP surface against side reactions with the electrolyte, including HF that is considered to be the main factor responsible for LCP degradation on cycling.[12, 25] Furthermore metal-fluorine bonding could also improve the crystal structure stability.[26, 27]

Figure 5b shows the galvanostatic profile of the first cycle of the pristine LCP, LCP-F1 and LCP-F2 at 0.1 C within the potential window 3.5 – 5.0 V vs Li^+/Li. The initial charge/discharge capacities of LCP, LCP-F1 and LCP-F2 are 170/102, 182/117 and 166/104 mAh g^{-1}, with the initial Coulombic efficiency of 60, 64 and 63 %, respectively. The lower capacity of LCP-F2 compared to LCP-F1 might be explained by the fact that a deeper fluorination (31.0 at% as the total fluorine content vs 9.4 at% for LCP-F1) results in a deeper surface modification as shown in Figure 3, thus some LCP became electrochemically inactive with respect to Li ion insertion/disinsertion. Another interesting point in the galvanostatic profiles is that while the pristine LCP exhibits a smooth sloping discharge curve, LCP-F1 and LCP-F2 clearly show the presence of 2 plateaus at 4.8V and 4.7 V during discharge,[28,29] which is characteristic of the lithiation of LCP in two stages as described below.

$$CoPO_4 + 2/3\ Li^+ + 2/3\ e^- \rightarrow Li_{2/3}CoPO_4 \quad (1)$$

$$Li_{2/3}CoPO_4 + 1/3\ Li^+ + 1/3\ e^- \rightarrow LiCoPO_4 \quad (2)$$

This result indicates that the fluorination could reduce the surface resistance between LCP particles and the electrolyte, which is discussed in the electrochemical impedance spectroscopy section.

As shown in Figure 5c, the increase of polarization for LCP-F1 and LCP-F2 is suppressed compared to that of pristine LCP. LCP-F1 and LCP-F2, which both show much lower cell polarization of 0.08 V at the 2nd cycle, exhibit only an increase of 0.02 V up to the 10th cycle, while an increase of 0.06 V (from 0.12 to 0.18) was recorded for the pristine LCP.

The Coulombic efficiency, which is one of the most important parameters for the commercialization of electrode materials, shows the same trend as the cycling performance and the polarization. As shown in Figure 5d, both LCP-F1 and LCP-F2 display not only higher Coulombic efficiency than the pristine LCP in early cycles, but also a rapid stabilization reaching > 95 % after 10 cycles at 0.1 C, while 15 cycles were needed for the pristine LCP. Nevertheless, the Columbic efficiency remained only around 98% for subsequent cycles due to a continuous decomposition of LP30 electrolyte at high voltage. Figure 5e displays the rate performance of the LCP samples at various current densities from 0.1 C to 2 C. As current density increases, the capacity decrease became more important for the pristine LCP, for example only 8 mAh g^{-1} of discharge capacity was recorded at 0.5 C while LCP-F1 and LCP-F2 show 58 and 52 mAh g^{-1} at the same rate, respectively. Interestingly, despite the lower initial capacity of LCP-F2 compared to LCP-F1, both fluorinated LCP delivered the same capacity at 1C, which means that LCP-F2 is more efficient for capacity retention at high rate. (Figure S4 for normalized discharge capacity) Finally, the performance of surface fluorinated LCP samples was compared with the pristine LCP sample assembled with 5% of fluoroethylene carbonate (FEC) added to the electrolyte. Indeed, FEC is a common additive used for both negative and positive electrodes, enabling more stable solid electrolyte interphases (SEI) or cathode electrolyte interface (CEI).[18] As shown in Figure 5f, any positive effect was not observed for the pristine LCP with 5% FEC, while the performance became worse for LCP-F2 with 5% FEC. This result might suggest that at first, FEC as an electrolyte additive cannot stabilize the CEI, also that the direct surface fluorination was a more efficient method for surface stabilization with enhanced electrochemical performance.

The enhanced electrochemical performance of the fluorinated LCP compared to pristine LCP and pristine LCP with 5% FEC is further revealed by electrochemical impedance spectroscopy (EIS). As shown in Figure 6a, the Nyquist plots for LCP-F2 exhibits a depressed

single semicircle in the medium to high frequency range, which could be interpreted as the sum of the charge transfer resistance (Rct) between the electrolyte and LCP-F2 surface and cathode electrolyte interfacial resistance (CEI, Rsf) formed at the particle surface. The straight line in the low-frequency region can reflect bulk Li ion diffusion (Warburg impedance). Upon cycling, the semicircle slightly increases, indicating the increase of resistance as seen in the polarization (Figure 5c). In the case of pristine LCP (Figure 6b), the semicircle in the medium to high frequency range is almost invisible, giving only the presence of a hump with higher resistance. The charge transfer resistance estimated using Nyquist plots fitting is 927, 2820 and 3005 Ohm for LCP-F2, pristine LCP and pristine LCP with 5% FEC in the electrolyte. The Nyquist plots for LCP-FEC (Figure 6c) are very similar to those of the pristine LCP, which confirm again that 5% FEC in the electrolyte is not efficient enough to stabilize the particle surface.

3. Conclusion

In summary, surface-fluorinated LCP materials have been successfully prepared by a one-step facile and dry method at room temperature using XeF_2 as fluorine source. After fluorination, fluorine-rich nanoparticles were observed mainly on the particle surface, as shown using SEM and STEM coupled with energy dispersive X-ray (EDX) spectra.

The half coin cell test for fluorinated LCP showed much improved cycling performance at 0.1 C, compared to the pristine LCP, along with a decrease of the polarization. This result could imply that the fluorine at the surface can stabilize the surface, especially by protection of the LCP surface against side reactions with electrolyte, such as surface degradation (amorphization) by HF attack. More importantly, the direct surface fluorination proved more efficient than adding fluorinated electrolyte additive (i.e. FEC), as demonstrated by electrochemical impedance spectroscopy. It is clear that the surface fluorination using XeF_2 is

a one-step, room temperature processable dry method to easily improve the performance of high voltage positive electrode materials for lithium ion batteries.

4. Experimental Section

Preparation of $LiCoPO_4$ (LCP): Samples were synthesized by a solvothermal method previously reported by Brutti and coworkers with slight modification.[21,30] Two aqueous solutions: solution A with lithium hydroxide monohydrate ($LiOH \cdot H_2O$, Sigma-Aldrich, ≥ 98 %) and solution B containing lithium dihydrogen phosphate (LiH_2PO_4, Alfa Aesar, 97 %), cobalt sulfate heptahydrate ($CoSO_4 \cdot 7H_2O$, Sigma-Aldrich, ≥ 99 %), and D-(+)-glucose (Sigma-Aldrich) were prepared separately. The solution A was added to ethylene glycol to give solution C. Subsequently the solution B was added dropwise into the solution C under stirring. The molar ratio of $LiOH\ H_2O$:$CoSO_4\ 7H_2O$:LiH_2PO_4 : D-(+)-glucose was 1.75 : 1 : 1 : 0.03. The Co^{2+} concentration in the final ethylene glycol/water solution was 0.1 M. The obtained purple suspension was sealed in a 135 ml Teflon-lined autoclave and heated in an oven at 220 °C for 16 h. The product was filtered, washed with water and ethanol then dried at 80 °C.

Fluorination of LCP: Fluorination of LCP was carried out using Xenon difluoride (XeF_2, Sigma-Aldrich, 99.99 %) as F source. Briefly, 300 mg of LCP was placed in a polytetrafluoroethylene (PTFE) reactor, in which a PTFE crucible containing 24 mg of XeF_2 was placed. Afterwards, the reactor was closed with the cap, then kept for 1h30 (LCP-F1) or 3h30 (LCP-F2), respectively. All experiments were performed in an Ar-filled glove box. Temperature and pressure for fluorination were RT and 1 atm.

Characterization: Powder X-ray diffraction (PXRD) patterns of samples were collected on a PANalytical Empyrean diffractometer operating in transmission mode with Mo $K\alpha_{1,2}$ radiation (λ = 0.7107 Å). Samples were loaded in a 0.7 mm glass capillary in an Ar-filled glovebox, sealed with vacuum grease. During the measurement, the capillary was spun to

reduce preferred orientation effects. Lattice parameters were obtained by the Le Bail method using the GSAS package with the EXPGUI interface.[31] Scanning electron microscopy (SEM) images were acquired with a Hitachi S-4800 electron microscope. Scanning transmission electron microscope (STEM) images were taken using a FEI Titan Themis 200 and Energy dispersive X-ray spectroscopy (EDS) spectra was collected with a Super-X high sensitivity windowless EDX detector. Magnetic susceptibility data were collected with a Quantum Design MPMS-XL SQUID magnetometer working in the range 2–300 K with the magnetic field up to 7 Tesla.

XPS analysis were carried out by the mean of an ESCALAB 250 Xi spectrometer with a monochromatic Al-Kα X-ray source (hυ = 1486.6 eV) probing between 5 to 10 nm of the surface (~95% of the signal is originating from the first 5 nm). The analysis of a 400×400 mm² area of the sample was done employing 20 eV as pass energy and 0.1 eV as energy step for the core peaks. Electron flood gun was used for charge compensation. The quantifications were done using CASA XPS software, after Shirley-type background subtraction, by utilizing the Thermo Fisher Scientific Advantage cross-section database. The apparatus was directly connected to a glovebox, allowing us to transfer the powders under argon inert atmosphere with oxygen and moisture under 0.5 ppm.

Galvanostatic electrochemical characterizations were performed at RT on a BTS3000 instrument (Neware Battery). Electrochemical impedance spectroscopy (EIS) studies were carried out on a VSP (BioLogic), from 100 kHz to 10 mHz, with a 10 mV amplitude in the potentiostatic mode. The electrodes are composed of the active material, a conductive carbon additive (Super C65), and polyvinylidene fluoride (PVDF, Solef 5130) in the mass ratio of 75:15:10. After stirring in N-methyl-2-pyrrolidone (NMP, Sigma-Aldrich), the electrode slurry was mixed in an agate grinding jar (1 h at 500 rpm), then tape cast uniformly at 150 um onto an aluminum current collector (0.018 mm, 99.0%, Goodfellow) using a 3540 bird film applicator (Elcometer). Electrodes were cut out from the film (diameter of 12.7 mm) and

dried under vacuum at 80 °C for 15 h. CR2032 coin-type cells were assembled in a glove box (MBraun) under Ar atmosphere (O_2 < 0.5 ppm, H_2O < 0.5 ppm), using lithium metal as both reference and counter electrode. The electrolyte was LP30 (1M $LiPF_6$ in ethylene carbonate (EC) and dimethyl carbonate (DMC) (w/w = 1:1)). Whatman glass fibre disks were used as separators. Typical electrode loadings were 2.5 mg cm^{-2}, with a thickness of ca. 15 µm. Electrochemical galvanostatic cycling was performed in the voltage window 3.5 - 5.0 V vs Li^+/Li at several different current densities.

Supporting Information
Supporting Information is available from the Wiley Online Library or from the author.

Acknowledgements
EJK would like to thank the Alistore ERI for the award of a studentship. The authors thank EPSRC Capital for Great Technologies Grant EP/L017008/1. The authors want to thank the French Research Network on the Electrochemical Energy Storage (RS2E) for YCB's PhD grant. MD and NL are indebted to the IR-RMN-THC FR3050 CNRS for the spectrometer time access and the financial support of the NMR experiments.

Received: ((will be filled in by the editorial staff))
Revised: ((will be filled in by the editorial staff))
Published online: ((will be filled in by the editorial staff))

References

[1] M. Armand and J. M. Tarascon, *Nature*, **2008**, 451, 652.

[2] V. Etacheri, R. Marom, R. Elazari, G. Salitra and D. Aurbach, *Energy Environ. Sci.*, **2011**, 4, 3243.

[3] W. Li, B. Song and A. Manthiram, *Chem. Soc. Rev.*, **2017**, 46, 3006–3059.

[4] K. Xu, *Chem. Rev.*, **2004**, 104, 4303.

[5] D. Aurbach, B. Markovsky, G. Salitra, E. Markevich, Y. Talyossef, M. Koltypin, L. Nazar, B. Ellis and D. Kovacheva, *J. Power Sources*, **2007**, 165, 491.

[6] W. Zhao, J. Zheng, L. Zou, H. Jia, B. Liu, H. Wang, M. H. Engelhard, C. Wang, W. Xu, Y. Yang and J.-G. Zhang, *Adv. Energy Mater.*, **2018**, 8, 1800297.

[7] J.-N. Zhang, Q. Li, Y. Wang, J. Zheng, X. Yu and H. Li, *Energy Storage Materials*, **2019**, 14, 1.

[8] D. Sun, Q. Wang, J. Zhou, Y. Lyu, Y. Liu and B. Guo, *J. Electrochem. Soc.*, **2018**, 165, A2032.

[9] S. Kalluri, M. Yoon, M. Jo, S. Park, S. Myeong, J. Kim, S.-X. Dou, Z. Guo and J. Cho, *Adv. Energy Mater.*, **2016**, 7, 1601507.

[10] K. Amine, *Electrochem. Solid-State Lett.*, **1999**, 3, 178.

[11] R. Sharabi, E. Markevich, K. Fridman, G. Gershinsky, G. Salitra, D. Aurbach, G. Semrau, M. A. Schmidt, N. Schall and C. Bruenig, *Electrochem. Commun.*, **2013**, 28, 20.

[12] E. Markevich, R. Sharabi, H. Gottlieb, V. Borgel, K. Fridman, G. Salitra, D. Aurbach, G. Semrau, M. A. Schmidt, N. Schall and C. Bruenig, *Electrochem. Commun.*, **2012**, 15, 22.

[13] Y. H. Ikuhara, X. Gao, C. A. J. Fisher, A. Kuwabara, H. Moriwake, K. Kohama, H. Iba and Y. Ikuhara, *J. Mater. Chem. A*, **2017**, 5, 9329.

[14] Q. D. Truong, M. K. Devaraju, Y. Sasaki, H. Hyodo, T. Tomai and I. Honma, *Chem. Mater.*, **2014**, 26, 2770.

[15] E. J. Kim, D. N. Miller, J. T. S. Irvine, A. R. Armstrong, *Chemelectrochem*, **2019**, 6, 4885.

[16] N. Laszczynski, A. Birrozzi, K. Maranski, M. Copley, M. E. Schuster and S. Passerini, *J. Mater. Chem. A*, **2016**, 4, 17121.

[17] B. Wu, H. Xu, D. Mu, L. Shi, B. Jiang, L. Gai, L. Wang, Q. Liu, L. Ben and F. Wu, *J. Power Sources*, **2016**, 304, 181.

[18] E. Markevich, G. Salitra and D. Aurbach, *ACS Energy Lett.*, **2017**, 2, 1337–1345.

[19] Y. Wang, H. Ming, J. Qiu, Z. Yu, M. Li, S. Zhang and Y. Yang, *J. Electroanal. Chem.*, **2017**, 802, 8.

[20] R. Sharabi, E. Markevich, V. Borgel, G. Salitra, D. Aurbach, G. Semrau, M. A. Schmidt, N. Schall and C. Stinner, *Electrochem. Commun.*, **2011**, 13, 800–802.

[21] E. J. Kim, X. Yue, J. T. S. Irvine and A. R. Armstrong, *J. Power Sources*, **2018**, 403, 11.

[22] H. Yang, P. Liu, Q. Chen, X. Liu, Y. Lu, S. Xie, L. Ni, X. Wu, M. Peng, Y. Chen, Y. Tang and Y. Chen, *RSC Adv.*, **2014**, 4, 35522.

[23] J. Ludwig, C. Marino, D. Haering, C. Stinner, D. Nordlund, M. M. Doeff, H. A. Gasteiger and T. Nilges, *RSC Adv.*, **2016**, 6, 82984.

[24] J. Ludwig, C. Marino, D. Haering, C. Stinner, H. A. Gasteiger and T. Nilges, *J. Power Sources*, **2017**, 342, 214.

[25] M. Zhang, N. Garcia-Araez, A. L. Hector, J. Mater. Chem. A, **2018**, 6, 14483.

[26] G. Du, Y. NuLi, J. Yang, J. Wang, Mater. Res. **2008**, 43, 3607.

[27] S. K. Kumar, S. Ghosh, P. Ghosal, S. K. Martha, J. Power Sources, **2017**, 356, 115.

[28] N. N. Bramnik, K. Nikolowski, C. Baehtz, K. G. Bramnik and H. Ehrenberg, *Chem. Mater.*, **2007**, 19, 908–915.

[29] F. C. Strobridge, R. J. Clément, M. Leskes, D. S. Middlemiss, O. J. Borkiewicz, K. M. Wiaderek, K. W. Chapman, P. J. Chupas and C. P. Grey, *Chem. Mater.*, **2014**, 26, 6193.

[30] J. Manzi, M. Curcio and S. Brutti, *Nanomaterials*, **2015**, 5, 2212.

[31] B. H. Toby, *J Appl Crystallogr*, **2001**, 34, 210.

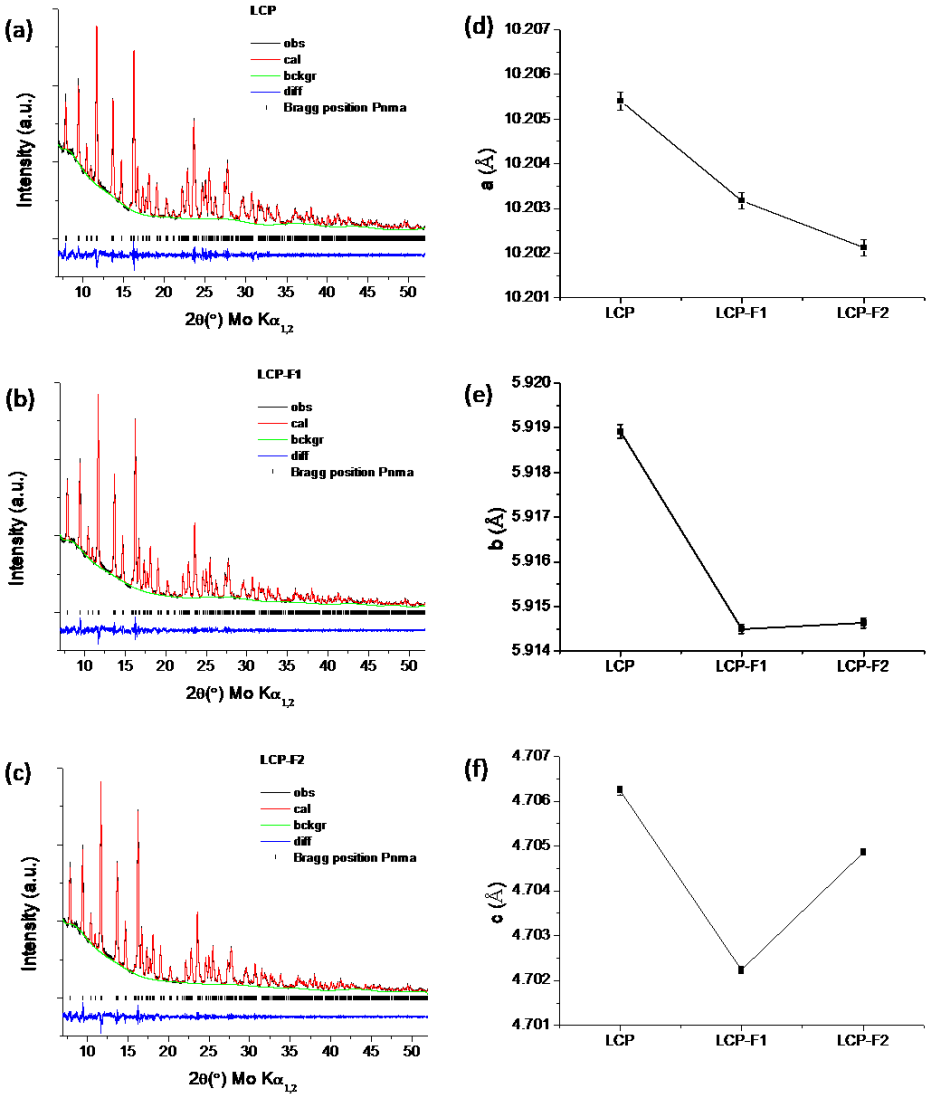

Figure 1. Profile fits for powder XRD patterns of (a) LCP, (b) LCP-F1 and (c) LCP-F2 using the Le Bail method. Observed data points are shown in black, with a fitted profile in red and the difference is shown in blue. Tick marks indicate allowed reflections. Refined cell parameters of (d) a, (e) b and (f) c.

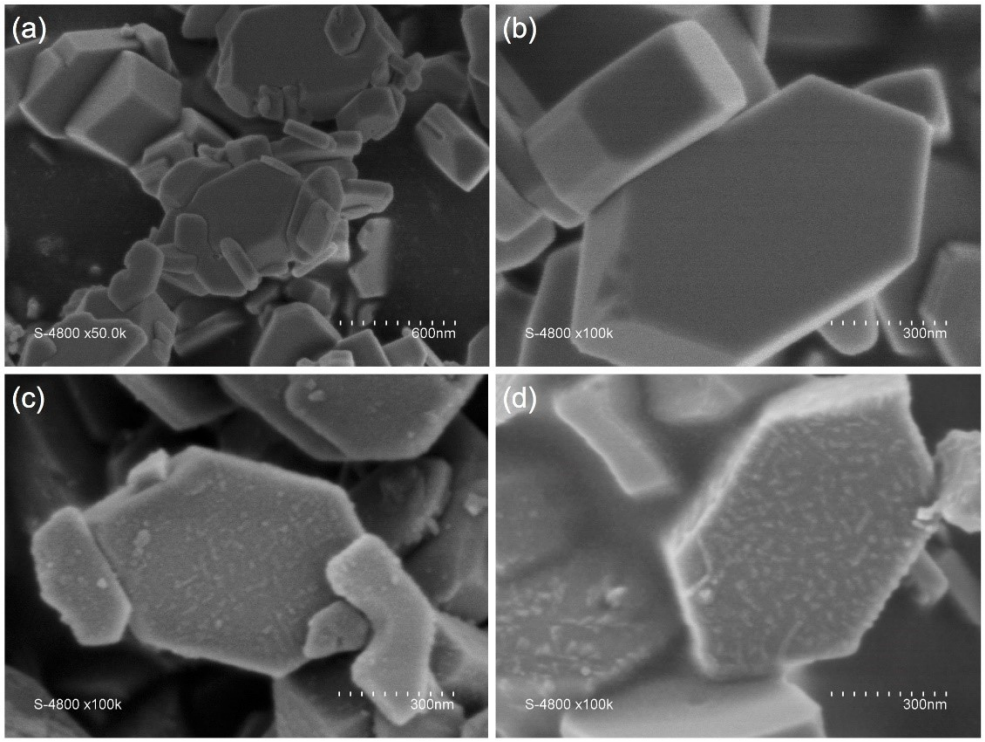

Figure 2. SEM images of a-b) the pristine LCP, b) LCP-F1 and c) LCP-F2

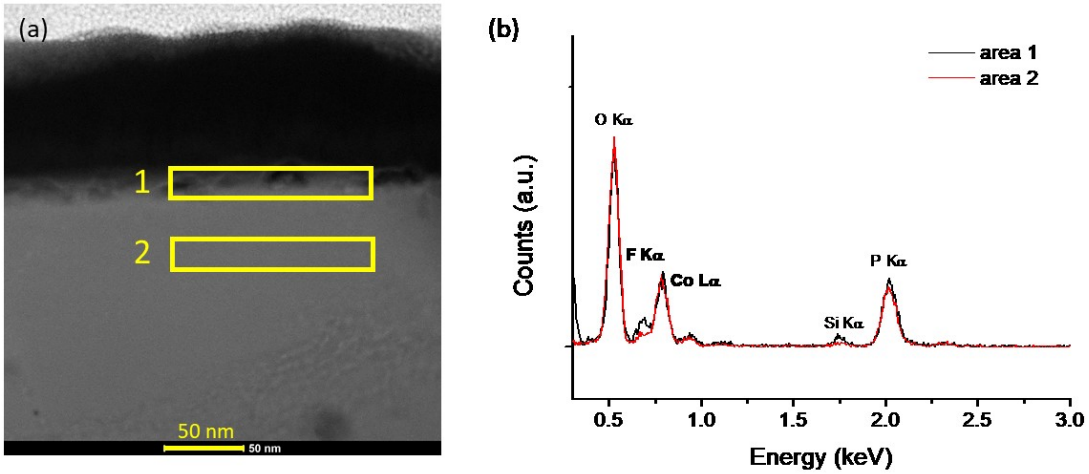

Figure 3. a) STEM image of LCP-F2, with surface coated with carbon and platinum (upper side of zone 1, b) EDX spectra of selected zones.

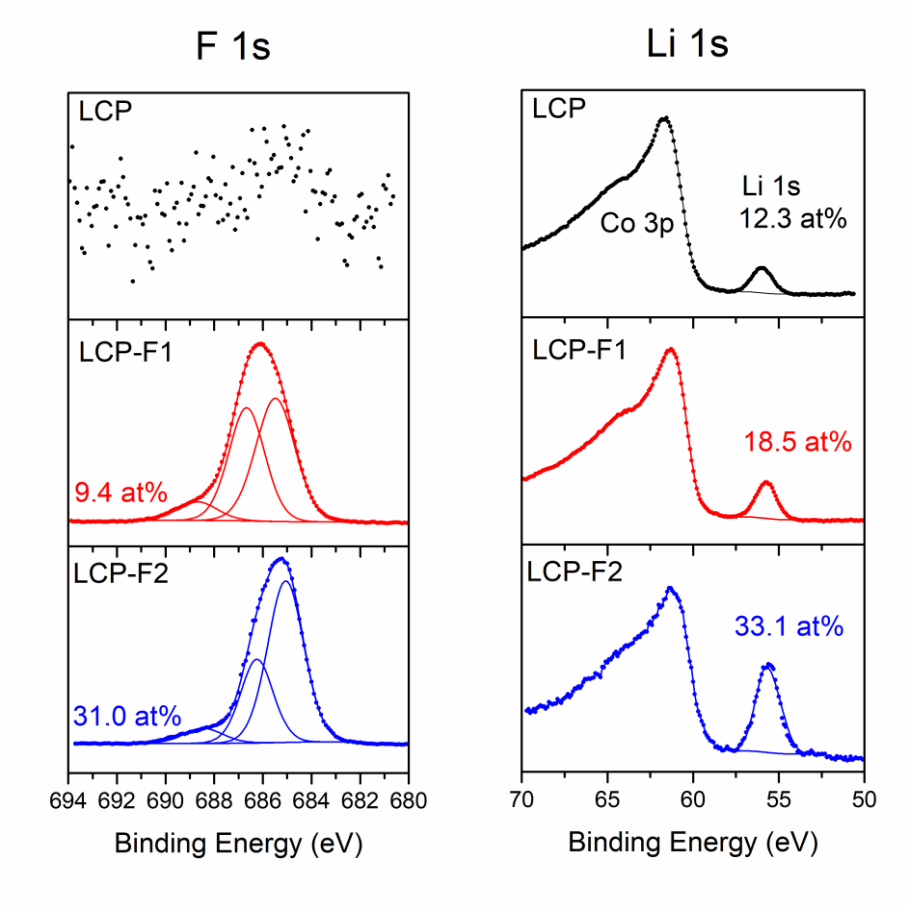

Figure 4. XPS high resolution spectra of F1s and Li1s for LCP, LCP-F1 and LCP-F2

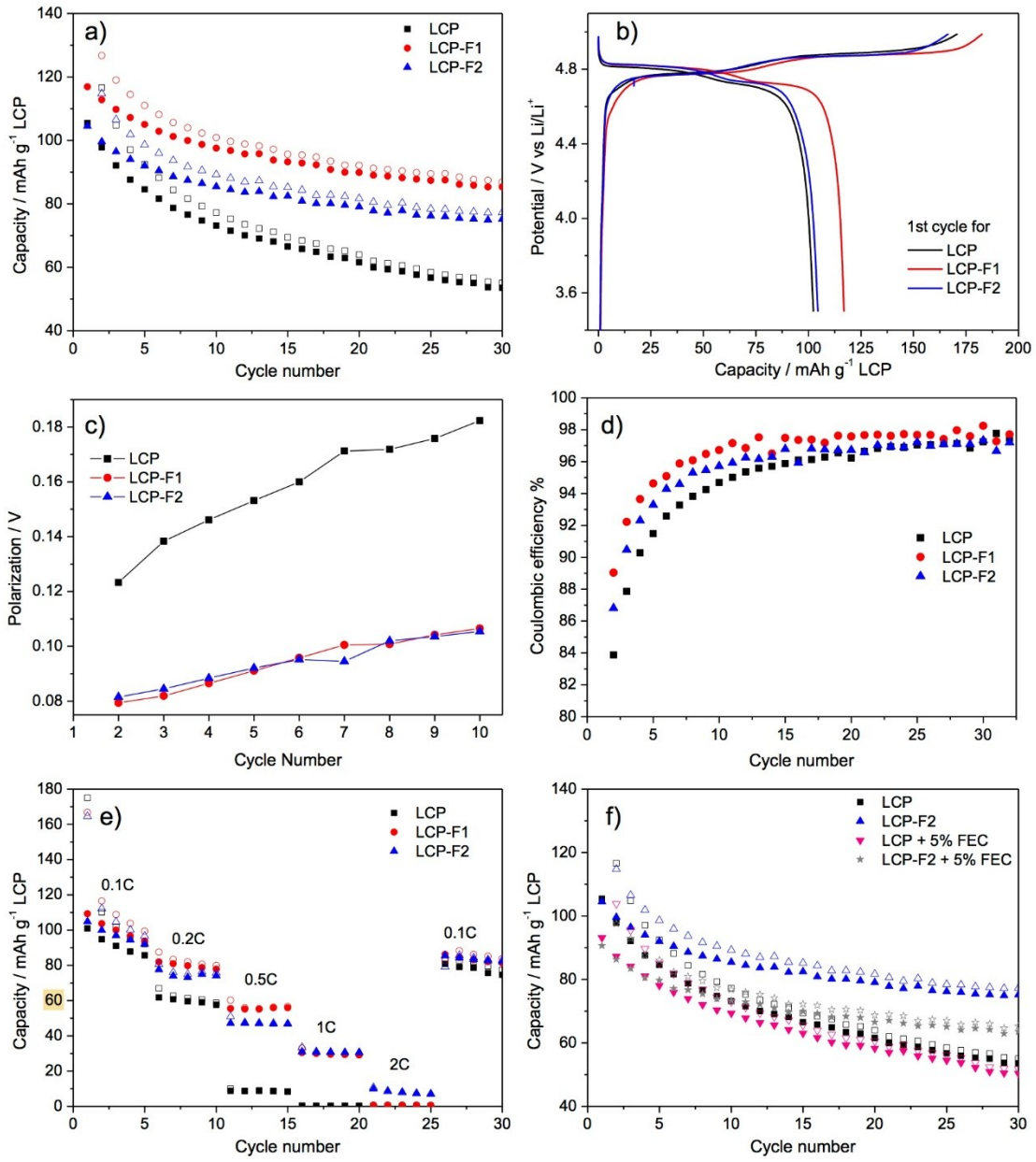

Figure 5. Electrochemical performance of the pristine LCP, LCP-F1 and LCP-F2; a) long term cyclability at 0.1 C (16.7 mA g^{-1}), b) Galvanostatic profile at 1st cycle at 0.1 C, c) Polarization as a function of cycle number, d) Coulombic efficiency, e) C-Rate performance and f) Comparison with 5% FEC added electrolyte. Open symbols stand for charge capacity and filled symbols for discharge capacity. Long term cyclability result with the error bar can be found in Figure S5.

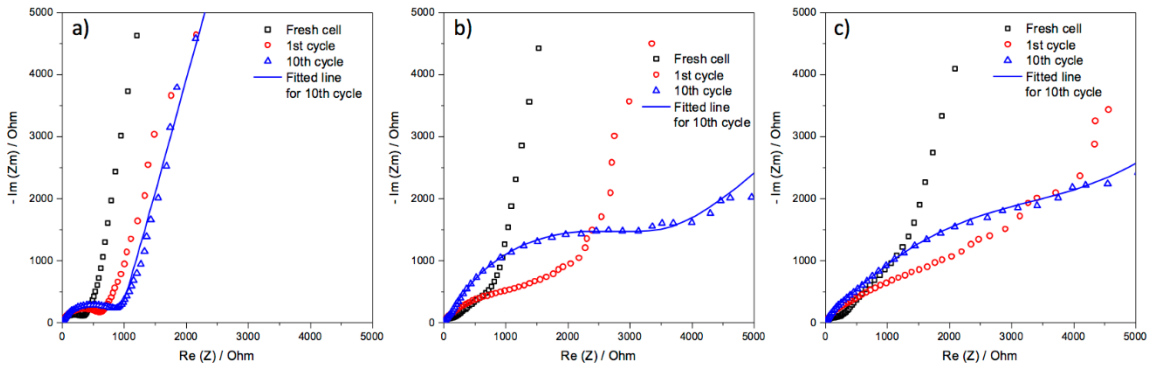

Figure 6. Nyquist plots of a) LCP-F2, b) the pristine LCP and c) the pristine LCP with 5% FEC in the electrolyte. Equivalent circuit used, and fitting parameters can be found in Table S2.

The electrochemical performance of 5V class positive electrode material lithium cobalt phosphate (LCP) is improved by atomic layer fluorination, which leads to the formation of Co-F nanoparticles at the surface. The fluorinated surface suppress the continuous electrolyte decomposition > 4.5 V, enabling the formation of a stable passivation layer formation, which is the key of better durability over cycling.

Keyword *LCP, fluorination, X-ray photoelectron spectroscopy (XPS), lithium ion battery*

*Sanghoon Kim, Eun Jeong Kim, Youn Charles-Blin, Katia Guérin, Marc Dubois, Delphine Flahaut, Herve Martinez, Michaël Deschamps, David N. Miller, John T.S. Irvine, A. Robert Armstrong, Laure Monconduit, and Nicolas Louvain**

Title *Atomic layer fluorination of 5 V class positive electrode material LiCoPO4 for enhanced electrochemical performance*